Plant Physiology and Biochemistry 216 (2024) 109198

Contents lists available at ScienceDirect

Plant Physiology and Biochemistry

journal homepage: www.elsevier.com/locate/plaphy

# Unravelling the physiological and molecular mechanisms of leaf color change in *Acer griseum* through multi-omics analysis

Huizhen Fan [a], Huimin Liao [a], Yingxue Shen [a], Md Nasir Hossain Sani [b,*], Jean Wan Hong Yong [b], Junyang Song [a,b,**]

[a] College of Landscape Architecture and Art, Northwest A&F University (NWAFU), 712100, Yangling, China
[b] Department of Biosystems and Technology, Swedish University of Agricultural Sciences (SLU), 234 56, Alnarp, Sweden

ARTICLE INFO

Handling Editor: Shivendra Sahi

*Keywords:*
*Acer griseum*
Leaf color variation
Anthocyanidins
Metabolomics
Transcriptomics
Genetic breeding

ABSTRACT

Paperbark maple (*Acer griseum*), an endemic and endangered wild plant in China, has red-colored autumn leaves of high ornamental and garden application value. Leaf color change serves as a crucial indicator for evaluating garden tree aesthetics; however, research on *A. griseum's* leaf color change remains limited. This study aims to elucidate the physiological and molecular mechanisms underlying leaf color change in maple leaves through physiological, transcriptional, and metabolic assays. Data analysis encompasses gene expression levels and metabolite changes in three distinct states of maple leaves: green, half-red, and red. The progessive decrease of chlorophyll and carotenoids and the continuous accumulation of anthocyanidins caused a sharp change in leaf coloration, which was most drastic in the green to half-red period. Subsequently, targeted metabolomics analysis was performed, and a total of 71 anthocyanidins were detected, and the content of eight types of anthocyanidins increased significantly in the half-red and red periods, compared with that in the green period; of which the multiplicative difference was the largest for cyanidin-3,5-O diglucoside, delivering the largest multiplicative difference. Thus, it was plausible that cyanidin-3,5-O-diglucoside-dominated compoundswere likely to be the main metabolites associated with leaf reddening. Correlation analysis revealed that 12 key transcription factors (TFs) were significantly correlated with the anthocyanin-related metabolites and structural genes, which play important regulatory roles during the biosynthesis of anthocyanosides in *A. griseum*. These findings offered useful insights into the molecular basis of leaf color variation in *A. griseum*; providing valuable information to guide targeted genetic breeding and varietal improvement strategies.

## 1. Introduction

Maple trees, belonging to the genus *Acer*, are esteemed for their aesthetic appeal, and are frequently utilized in landscape adornment. Renowned for their seasonally shifting leaf colors, they are highly valued for their ornamental attributes. The genus *Acer* encompasses over 200 species, primarily distributed across temperate regions spanning Asia, Europe, and America. Paperbark maple (*Acer griseum* Franch.) Pax, a member of the *Acer* genus within the Sapindaceae family, stands as an endemic and endangered species indigenous to China (Gibbs and Chen, 2009). Exhibiting characteristic autumnal foliage, adorned with hues of ochre-red, *Acer griseum* epitomizes the superior ornamental traits emblematic of the maple family. Its captivating foliage, complemented by its distinctive ochre-red trunk, contributes to the resplendent autumnal landscape, solidifying its status as an esteemed species for landscaping endeavors. Thus, the dynamic alterations in leaf coloration during seasonal transitions in *Acer griseum* are an emblematic feature cherished by horticulturists and nature enthusiasts alike.

As part of foliar photosynthesis, leaves play an important role in the growth and development of plants. Coloration varies among the different colored-leaf species, and their photosynthetic capacity is generally altered accordingly because of the changes in various pigment content (Menzies et al., 2016). During photosynthesis in general, the absorption, transfer, and conversion of light energy take place in the chloroplasts of most higher plants (Ma et al., 2021; Walter and Kromdijk, 2022). Conversely, in species with colored leaves, the structures of chloroplasts are often altered. Interestingly, the general mechanisms governing changes in leaf coloration are probably multi-fold, and

* Corresponding author.
** Corresponding author. College of Landscape Architecture and Art, Northwest A&F University (NWAFU), 712100, Yangling, China.
*E-mail addresses:* md.sani@slu.se (M.N.H. Sani), songjunyang@nwafu.edu.cn (J. Song).

https://doi.org/10.1016/j.plaphy.2024.109198
Received 26 July 2024; Received in revised form 29 September 2024; Accepted 12 October 2024
Available online 16 October 2024

complex (Chen et al., 2017; Hughes and Lev-Yadun, 2023; Lev-Yadun, 2022; Li et al., 2022; Sheue et al., 2007). Throughout seasonal foliar color changes, leaves undergo significant biochemical alterations, including shifts in chlorophyll, carotenoids, and anthocyanin content and distribution (Menzies et al., 2016; Winkel-Shirley, 2001). Previous studies have shown that changes in the content of natural pigments such as chlorophyll, carotenoid and anthocyanin are the determining factors affecting the formation of leaf colour in vibrant foliage plants (Alappat and Alappat, 2020; Li et al., 2022). Among these pigments, the accumulation of anthocyanin content is a key factor contributing to the purplish red colour of leaves (Chen et al., 2019). Anthocyanin is a natural, water-soluble pigment widely found in plant stems (Gao et al., 2020), leaves (Duan et al., 2023), flowers and fruits (Espley and Jaakola, 2023; Karppinen et al., 2021). Beyond its ornamental significance, anthocyanin plays pivotal roles in pollination and fertilization (Zhu et al., 2023), and plant responses to various abiotic and biotic stresses (Naing and Kim, 2021; Qin et al., 2021), such as drought stress (An et al., 2020), salt stress (Li et al., 2022), low-temperature stress (Xu et al., 2023), disease infestation (Long et al., 2019), and other aspects.

Numerous anthocyanin glycosides have been identified in nature, with the most prevalent anthocyanins classes are (6 classes) pelargonidin (Pg), cyanidin (Cy), delphinidin (Dp), peonidin (Pn), petunidin (Pt), and malvidin (Mv) (He et al., 2010). Recent research has provided a deeper understanding of the anthocyanin synthesis pathway, particularly in plants such as cotton (Shao et al., 2021), and purple wheat (Wang et al., 2021). Anthocyanin biosynthesis initiates with the phenylpropanoid biosynthetic pathway (Liu et al., 2018). Subsequently, chalcone synthase (CHS) catalyzes the formation of yellow chalcone, which serves as a precursor for dihydroquercetin and dihydromyricetin flavonoids, essential intermediates in anthocyanin synthesis (Shi and Xie, 2014). The final stage encompasses the generation of various anthocyanins, which are eventually converted into stable anthocyanidins. Anthocyanin synthesis is mainly controlled by structural (Hong et al., 2016; Kim et al., 2018; Muhammad et al., 2022) and regulatory genes (He et al., 2023; Hong et al., 2016; Li et al., 2020). Additionally, other factors, including microRNA (Liu et al., 2017, 2023), light (Yan et al., 2023; Zhang et al., 2022, 2023), phytohormones (An et al., 2018; Li et al., 2024), and sugar signaling (Chen et al., 2017), exert influence on anthocyanin synthesis.

The synthesis, transport, and accumulation of anthocyanins are intricately regulated by a network of transcription factors, with particular emphasis on the MYB, bHLH, and WD40 families (Morita et al., 2006). These transcription factors play pivotal roles in orchestrating the expression of genes involved in the anthocyanin synthesis pathway. It is understood that these transcription factors can exert either promoting or inhibitory effects on anthocyanin biosynthesis by binding to specific regions within the promoters of structural genes (Shan et al., 2019). Additionally, they can form heterotrimeric complexes known as the MYB-bHLH-WD40 (MBW) complex, which acts synergistically to regulate the transcriptional activity of anthocyanin synthesis genes (Morita et al., 2006). Understanding the intricate regulation of anthocyanin synthesis by transcription factors and how these transcription factors coordinate the expression of anthocyanin synthesis genes forming complex regulatory networks is essential for unraveling the molecular mechanisms underlying plant pigmentation.

Recent advancements in high-throughput profiling and multi-omics technologies of botanicals have revolutionized our ability to dissect the molecular components of biological processes with unprecedented precision (Chang et al., 2011; Ge et al., 2008; Heng et al., 2013; Teo et al., 2011). Integration of genomics, transcriptomics, and metabolomics, data provides a comprehensive framework for understanding the intricate networks governing leaf color variation. Several recent studies have demonstrated the power of multi-omics analysis in deciphering complex biological processes in plants (Azarin et al., 2024; Chen et al., 2017; Feng et al., 2024; He et al., 2023; Ma et al., 2022). For instance, next-generation high-throughput sequencing technology has been widely used in various ornamental plants in recent years, such as *Camellia japonica* (Fu et al., 2021), *Liriodendron tulipifera* (Hao et al., 2020), red maple (Lu et al., 2020), which enrich the transcriptional data of ornamentals and provide a good basis for the study of their colour-presenting mechanism and species selection. These species have enriched the transcriptional data of ornamental plants and laid a good foundation for the study of their colour-presenting mechanism and variety selection.

Building upon these advancements, our study provided novel insights into understanding the molecular basis of leaf color variation in *A. griseum*, thereby contributing to our broader understanding of plant pigmentation and adaptation to changing environments. Through the integration of traditional physiological techniques and modern molecular biology approaches, we characterized the biochemical changes within the leaves during the colour transitions. Additionally, we identified the key substances or genes responsible for regulating leaf color change in maple species (*Acer griseum*). By advancing our knowledge of plant pigmentation at the molecular level, our study provided broader insights into understanding plant adaptations to changing environments for the endangered plant species*Acer griseum*.

## 2. Materials and methods

### 2.1. Plant material

Plant materials were obtained from adult robustly growing *A. griseum* (age 12, diameter at breast height of about 17 cm, tree height of about 7 m) in the Botanical Garden of Northwest A&F University (34°16′19.286″N，108°4′48.792″E), and the leaves were collected at 10 a.m. on 16 October (Green leaf period), 14 November (Half-red leaf period), and 24 November (Red leaf period), respectively, during the autumn in 2022. There was a significant difference in leaf colour between the three periods (Fig. 1A) Sample collected evenly in four directions, east, south, west and north of the canopy, selecting healthy leaves free of pests and diseases, which were quickly packed into collection tubes and plunged into liquid nitrogen after isolation, brought back to the laboratory and stored in a −80° refrigerator. There were three biological replicates in each period, and a total of nine tubes were collected in the three periods, labelled as 'Green-1, Green-2, Green-3, Half-red-1, Half-red-2, Half-red-3, Red-1, Red-2, Red-3', and the subsequent physiological, transcriptomic and metabolic groups were taken from the tubes in this grouping and replication. The following physiological, transcriptional, and metabolic groups were sequentially sampled from the test tubes in this grouping and replication manner.

### 2.2. Detection of physiological indicators of chlorophyll and anthocyanin content

Determination of chlorophyll and carotenoid content: *A. griseum* leaves (without veins) with a mass of about 0.1 g were weighed from each of the nine tubes of samples, placed in 15 ml of the extract solution (acetone: anhydrous ethanol = 1:1), and left to stand at room temperature in a dark place. after 24 h, the samples were centrifuged using a centrifuge at a speed of 6000 rpm for 2 min. After obvious delamination, 1 ml of supernatant was aspirated into a cuvette, zeroed with the extract, and the absorbance was measured at 470, 645, and 663 nm with a visible spectrophotometer (Hitachi Limited, Japan) and the data were recorded, respectively. The contents of chlorophylls and carotenoids were calculated (He et al., 2023; Mei et al., 2021). For the determination of anthocyanin content: 0.1 g of *A. griseum* leaves were weighed, remove leafy stems, and cut into small pieces, placed in 15 ml of 1% hydrochloric acid methanol solution, overnight in the dark at room temperature, centrifuged and the supernatant was aspirated. Absorbance was measured at 530, 620 and 650 nm using a visible spectrophotometer (Hitachi Limited, Japan) and anthocyanin content was calculated (Inácio et al., 2013).

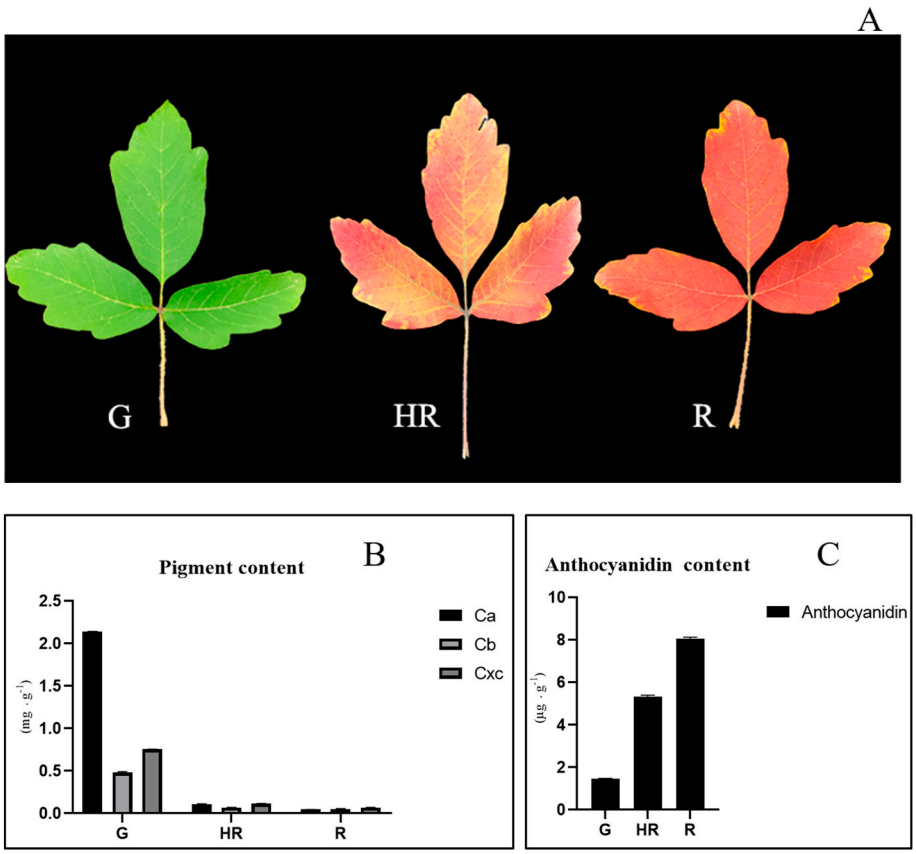


**Fig. 1.** Phenotypes of *A. griseum* leaves at three stages of discolouration and changes in chlorophyll, carotenoid, and anthocyanin content at each stage. A: phenotypic characteristics of *A. griseum* leaves at three stages of discolouration; B: changes in chlorophyll and carotenoid content, carotenoid content (mg/g) at three stages of discolouration of *A. griseum* leaves; C: Changes of anthocyanin content in three discolouration stages of *A. griseum* leaves, anthocyanin content (μg/g) Ca: chlorophyll *a*; Cb: chlorophyll *b*; Cxc: carotenoid; G: green leaf stage; HR: half-red leaf stage; R: red leaf stage.

### 2.3. Metabolite sample preparation and extract analysis, identification

After vacuum freeze-drying, the leaves of the *A. griseum* were ground (30 Hz, 1.5 min) to powder form, and 50 mg of the powder was weighed and dissolved with 500 μlL methanol/water/hydrochloric acid (500:500:1, V/V/V); vortexed for 5 min, ultrasonicated for 5 min, and centrifuged for 3 min (12, 000 r/min, 4 °C). The su-pernatants were filtrated with a 0.22 μm millipore filter, collected, andanalyzed using an UPLC-ESI-MS/MS system (UPLC, Exion LC™ AD; MS, Applied Bio-systems 6500 Triple Quadrupole) equipped an ESI TurboIon-Spray interface controlled by Analyst 1.6.3 software (AB Sciex). The steps and conditions of collection are as follows: UPLC: column, Waters ACQUITY BEH C18 (1.7 μm, 2.1 mm*100 mm); solvent system, water (0.1 % formic acid): methanol (0.1 % formic acid); gradient program, 95:5 V/V at 0 min, 50:50 V/V at 6 min, 5:95 V/V at 12 min, hold for 2 min, 95:5 V/V at 14 min; hold for 2 min; flow rate, 0.35 mL/min; temperature, 40 °C; injection volume, 2 μl. The ESI source operation parameters were as follows: ion source, ESI+; source temperature 550 °C; ion spray voltage (IS) 5500 V; curtain gas (CUR) was set at 35 psi, respectively. Data acquisitions were performed using Analyst 1.6.3 software (Sciex). Multiquant 3.0.3 software (Sciex) was used to quantify all metabolites. The identified metabolites were annotated, and results presented using a database (MetWare, https://www.metware.cn/) and the R package (heatmaply; ComplexHeatmap).

### 2.4. RNA extraction, cDNA library creation, transcriptome data analysis

The leaves were removed from the −80 °C ultra-low temperature refrigerator, quickly placed in liquid nitrogen, and total RNA was extracted from A. griseum according to the procedure in the kit (OMEGA E.Z.N.A Plant RNA kit).Briefly, mRNA was purified from total RNA using poly-T oligoattached magnetic beads. First strand cDNA was synthesized using random hexamer primer and M-MuLVReverse Transcriptase (RNase H-). Second strand cDNA synthesis was subsequently performed using DNA Polymerase I and RNase H. After selection of cDNA fragments of preferentially 250–300 bp in length with the AMPure XP system (Beckman Coulter, Beverly, USA), PCR was per-formed with Phusion High-Fidelity DNA polymerase, universal PCR primers, and index (X) primer. At last, PCR products were purified (AMPure XP system) and library quality was assessed on the Agilent Bioanalyzer 2100 system. The libraries were sequenced on the Illumina Novaseq platform to produce 150 bp paired end reads.

Next, the sequencing data were controlled for quality, and analyzed. Clean reads were obtained after filtering, checking, and cleaning the raw data using fastp. Transcriptome assembly was performed using Trinity. Corset was used to regroup relevant transcripts into 'gene' clusters (https://github.com/trinityrnaseq/trinityrnaseq). Use TransDecoder (https://github.com/TransDecoder/TransDecoder/wiki) to identify candidate coding regions within transcript sequences generated by de novo RNA-Seq transcript assembly using Trinity. Differential expression analysis between two groups of samples with biological replicates using DESeq2 R package (1.20.0). The *P* value was corrected using the Ben-jamini and Hochberg method. The corrected P value and |log2fold-change| are used as the threshold for significant difference expression. Differentially expressed genes were analyzed by GO, KEGG enrichment and other methods to obtain key pathways and genes.

### 2.5. Validation of transcriptome data by qRT-PCR

To verify the reliability of the transcriptome data, we selected 12

differential genes for qRT-PCR experiments. Primer Premier 5 software (http://www.premierbiosoft.) was used for specific primer design, and total RNA was reverse-transcribed into first-strand cDNA using the PrimeScript Reverse Transcriptase Kit (TaKaRa, Dalian, China). qRT-pcr experiments were performed using the StepOnePlusTM RT-PCR system and TransStart® Top Green qPCR SuperMix (+Dye I; M20105; TransGen Biotech, Beijing, China) for quantitative real-time PCR analysis. The total reaction system was 20 μl, including 0.8 μl each of upstream and downstream primers, 10 μl of enzyme, 8.2 μl of $ddH_2O$, and 1 μl of cDNA, and the amplification procedure was 95°C30S, 95°C10S, 60°C30S, and 45 cycles. Relative expression analysis was performed on the quantitative data using $2^{-\Delta\Delta Ct}$. Gene-specific primers used for qRT-PCR analysis are listed in Table S10. Three biological replicates and three technical replicates were performed for all experiments.

## 3. Results

### 3.1. Analysis of physiological indicators

In this study, the autumn leaf colour change of *A. griseum* was categorized into three stages: green (G), half-red (HR) and full red (R) as depicted in Fig. 1A. Analysis of leaf pigment content (Chlorophyll a, chlorophyll b, carotenoids, and anthocyanin glycoside) revealed distinct trends during these stages (Fig. 1B and **C**). However, Fig. 1-B demonstrated a decreasing trend in chlorophyll a, chlorophyll b, and carotenoids during leaf color changes, each with different rates of decline.

During the initial stage (G), chlorophyll a content was the highest (2.14 mg/g), with chlorophyll b (0.48 mg/g) and carotenoids (0.75 mg/g) lower but similar. The absolute dominance of chlorophyll a resulted in the green colour of the leaves in this stage. In the second stage (HR), the content of chlorophyll a decreased sharply (0.11 mg/g), and the content of chlorophyll b (0.07 mg/g) and carotenoids (0.12 mg/g) continued to decrease; as the leaves entered the third stage(R), the content of chlorophyll a (0.04 mg/g), chlorophyll b (0.05 mg/g) and carotenoids (0.07 mg/g) continued to decrease. The levels of chlorophyll a and chlorophyll b were lower both were basically flat; while the changes in the contents of total anthocyanin glycosides were diametrically opposite to their trends and showed an increasing trend, as shown in Fig. 1C, which sharply rising from the first stage (1.5 μg/g) to the second stage (5.3 μg/g), and continued to accumulate to the third stage (8.1 μg/g).These data suggest that a decrease in the content of chlorophyll a, chlorophyll b and carotenoids and a sustained increase in the content of anthocyanins may be the main reasons for the leaf discoloration.

During the process of leaf colour change, chlorophyll a, chlorophyll b, carotenoids, and total anthocyanin glycosides, changed significantly, showing two trends of change (decreasing type and increasing type). Chlorophyll a, chlorophyll b, and carotenoids were decreasing trends, and in the first to second stages, chlorophyll a, chlorophyll b, and carotenoids decreased by 95%, 85%, and 84%, respectively; in the second to third stages, chlorophyll a, chlorophyll b, and carotenoids decreased by 64%, 29%, and 42%, respectively. Concurrently, the content of total anthocyanosides was accumulating, and showed an ascending type of change trend, from the first to the third stage of a total of two interruptions, the content rose by 253% and 53%, respectively. The most significant disparity between both trends occurred during the transition from the first stage to the second stage, marking the shift from green to half-red leaves, a crucial period for *A. griseum* leaf color transformation. We anticipate that gene expression and metabolite synthesis related to this process would be particularly conspicuous during this stage.

### 3.2. Analysis of metabolomic data

To investigate the primary anthocyanidin fractions, we conducted metabolomic assays on leaves from three distinct periods, resulting in the identification of a total of 71 anthocyanins. These 71 anthocyanins fell into 8 major groups, namely 16 cyanidin, 11 peonidin, 10 delphinidin, 9 pelargonidin, 8 flavonoids, 7 malvidin, 6 petunidin, and 4 proanthocyanidins. Utilizing the metabolite contents across the three-color change stages, a clustering heat map was generated (Fig. 2), highlighting significant alterations during the transition from green to red leaves.

We classified these changes into three types: the first type of change was decreasing, such as Peonidin-3-sophoroside-5-glucoside, Peonidin-3-O-sophoroside, Malvidin-3-O-rutinoside, etc., which were higher in the green leaf period than in the half-red and full-red periods. It is presumed that metabolites with such trends are not the main metabolites causing reddening of leaves; the second group is the intermediate high type, such as Cyanidin-3,5-O-diglucoside, Cyanidin-3-O-(6-O-malonyl-beta-D-glucoside), Cyanidin-3-O- xyloside, etc. Their contents were highest in the half-red period, followed by the full red period, and lowest in the green period. In the period transitioning from green to half-red, the accumulation of metabolites with this kind was the most vigorous, contributing to a dominating role in the leaf colour change. Lastly, an ascending type, such as Delphinidin and Pelargonidin Malvidin-3-O-(6″-acetylglucoside)-5-glucoside, etc., demonstrated increasing levels, peaking during the full-red stage, implying their importance in the leaf reddening process.

To identify key metabolites, we compared the three stages of color change pairwise, creating three comparison groups (HRvsG, RvsG, RvsHR). Using fold change thresholds of $\geq 2$ and $\leq 0.5$, we screened for differential metabolites and visualized the data with clustered heatmaps and Venn diagrams (Fig. 3). The results showed that most of the metabolite accumulation was significantly higher in the later stages compared to the green period. HRvsG revealed 43 different metabolites (25 up-regulated and 18 down-regulated); RvsG showed 41 differential metabolites (23 up-regulated and 18 down-regulated); and RvsHR exhibited 9 different metabolites (1 up-regulated and 8 down-regulated). Differential anthocyanidins were classified into a total of eight groups, namely cyanidin, peonidin, pelargonidin, delphinidin, malvidin, petunidin, procyanidin, and flavonoid. Compared to the green period, the levels of cyanidin, pelargonidin, and flavonoid were more significantly elevated in the half-red and red periods, and cyanidin was the main up-regulated metabolite (Fig. 3A and B); whereas only one substance, malvidin-3-O-arabinoside, was up-regulated in RvsHR, and the rest were the most abundant in the semi-red period (Fig. 3C). According to the $\log_2$FC values of the metabolites in each group, Cyanidin-3,5-O-diglucoside was the most abundant metabolite in the green period, with a multiplicity of difference of 14.65 in the half-red period and 13.38 in the red period (Supplementary Fig. 1), which indicated that the changes of this metabolite varied the most significantly. Furthermore, it was the most abundant metabolite during the period from the green period to the half-red period. This indicates that the content of this metabolite varies most significantly and accumulates most vigorously in the green to half-red period, and that its changes is closely related to the coloration of the leaves. In the grouping comparison of differential metabolites (Fig. 3D), a total of 7 metabolites were present across all 3 periods, including 6 cyanidins (Cyanidin-3,5-O-diglucoside, Cyanidin-3-O-(6-O-malonyl-beta-D-glucoside),Cyanidin-3-O-arabinoside, Cyanidin-3-O-sophoroside,Cyanidin-3-O-xyloside,Cyanidin-3-O-sambubioside-5-O-glucoside) and a peonidin (Peonidin-3,5-O-diglucoside). It means that these anthocyanidins play a key role in leaf reddening.

### 3.3. Transcriptome data analysis

To investigate the molecular mechanism of anthocyanin biosynthesis during leaf colour change, we constructed 9 cDNA libraries (green, half-red and red, three biological replicates for each colour stage) for transcriptome analysis. Sequencing data were preprocessed to eliminate reads with splices and low quality, resulting in a total of 443,418,856 raw reads. After filtering, 413,382,296 clean reads remained. These clean reads were assembled using Trinity software tailored for high-throughput transcriptome sequencing. The splicing results showed

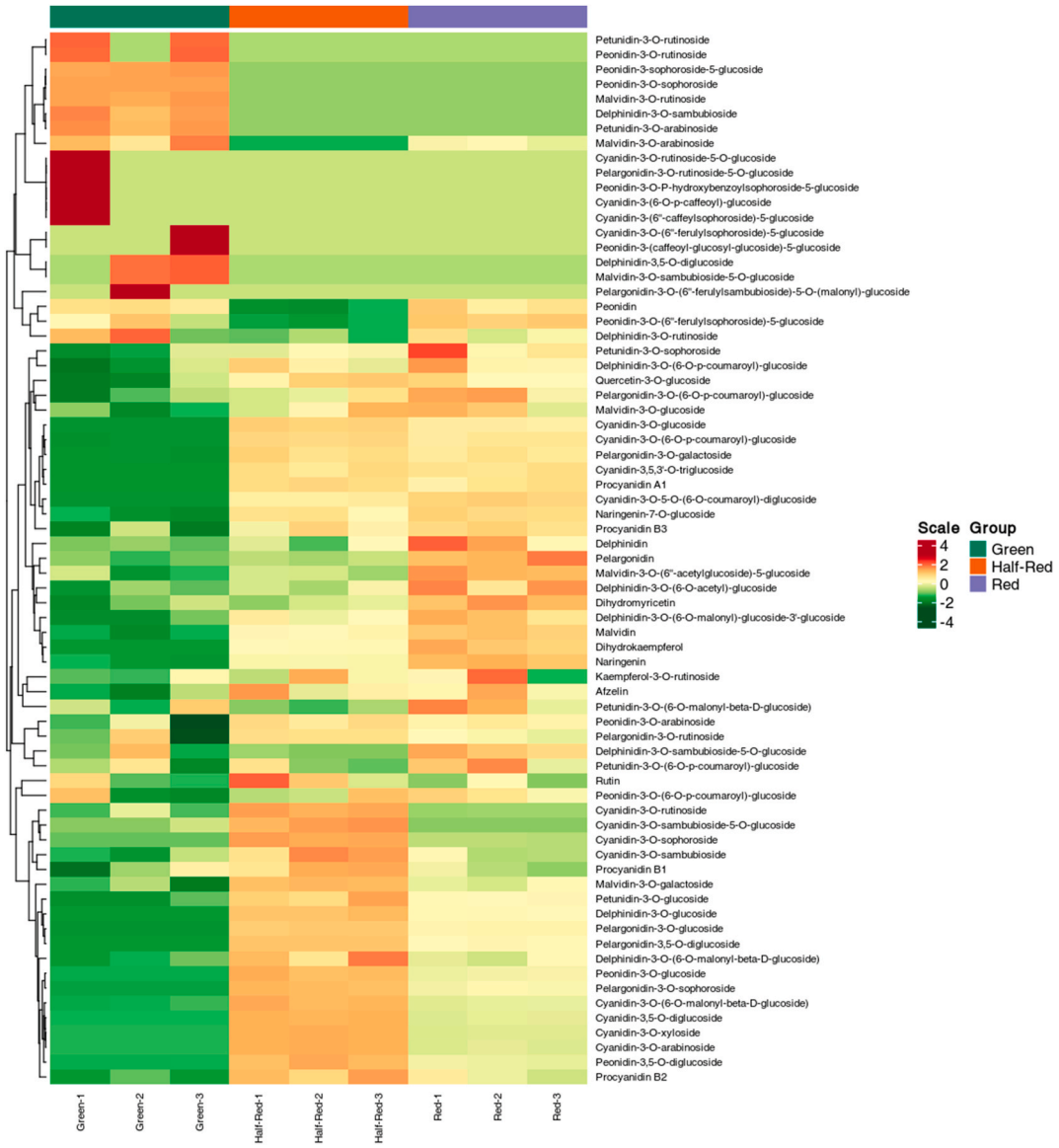


**Fig. 2.** Heatmap of metabolite clustering in three discoloration stages of *Acer griseum* leaves.

that the percentage of Q30 bases of each sample was 91.54% and above, and the percentage of GC content was 43.8% and above. A total of 157,632 Unigenes were obtained from the assembly, with a total length of 188,962,876 bp and an average length of 1199 bp. The N50 of the unigenes was 1856 bp, and the data indicated that the assembly integrity was high which could be used for subsequent analyses. Principal Component Analysis (PCA) of the samples revealed distinct dispersion between groups and tight aggregation within groups (Supplementary Fig. 2), suggesting that the leaves at different stages of discolouration were more different and biologically reproducible. To obtain annotation information for the differential genes, unigene sequences were aligned with KEGG, NR, Swiss-Prot, GO, COG/KOG, and Trembl databases, and all sequences were annotated.

### 3.4. Differential gene matching in different subgroups

To understand the transcriptomic features associated with *A. griseum* leaf color change, differential expression analysis was conducted using DESeq2 on three biological replicates of *A. griseum* leaves. Multiple hypothesis testing probability (P value) was corrected using the Benjamini-Hochberg method to obtain the False Discovery Rate (FDR). Applying filtering criteria of $|\log_2\text{Fold Change}| \geq 1$ and FDR $<0.05$, a total of 93,242 differential genes were identified. Specifically, 42,517 genes were differentially expressed between GvsHR, 47,643 between GvsR, and 3082 between HRvsR (Fig. 4A), with 1743 genes duplicated across all three groups (Fig. 4B). Annotation of the differential genes using KOG, GO, and KEGG databases revealed their involvement in various functions and pathways. Notably, a significant proportion of the differential genes were associated with General function prediction only and Posttranslational modification, protein turnover, chaperones (**KOG**, Supplementary Fig. 3). These genes played a significant role in diverse biological processes, as indicated by the GO database (Supplementary Fig. 4). The KEGG database showed that these differential genes were significantly enriched in metabolic pathways and secondary metabolite biosynthesis (Supplementary Fig. 5). Notably, the phenylpropanoid and flavonoid pathways, which are related to anthocyanin biosynthesis, were also labelled in the multi-combination KEGG enrichment scatter plots (Fig. 4C), and they were more enriched in the GvsHR and GvsR combinations, indicating that such metabolisms are more vigorous in the first half of the leaf's reddening phase, aligning with the results of previous phenotypic and physiological indicator assays (Fig. 1).

Additionally, the concatenated set of all differential gene FPKMs was

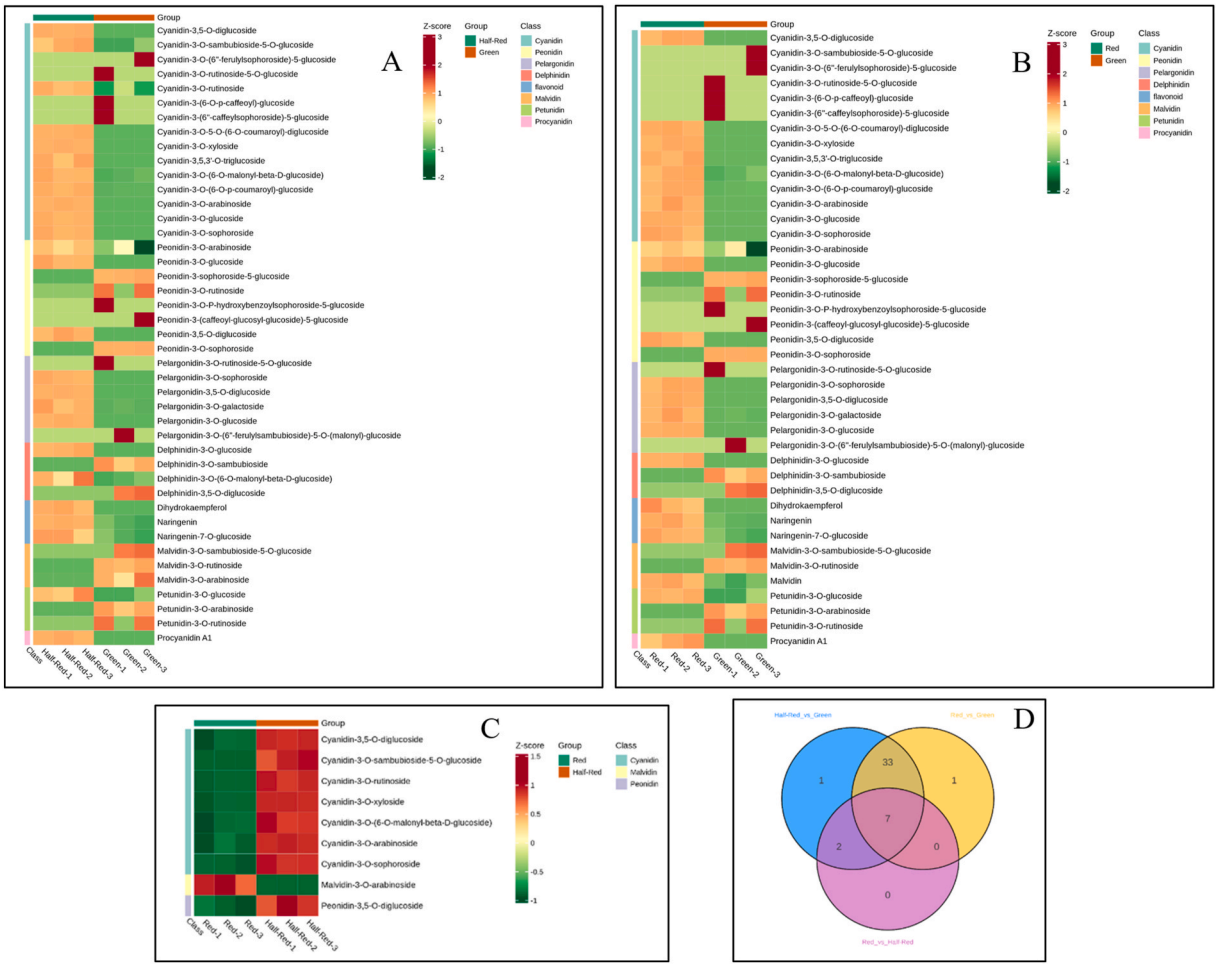


**Fig. 3.** Differences in the expression levels of metabolites in three discolouration stages of *A. griseum* leaves. **A-C**: heatmaps of anthocyanin expression levels in the three comparative groups (A,HRvsG; B,RvsG; C,RvsHR); **D**: Venn diagrams of metabolites in the three comparative groups.

normalized and subjected to Kmeans cluster analysis, resulting in classification into 10 clusters (Fig. 5A), broadly grouped into 3 expression trend types. The first type belonged to the ascending type, with four clusters, namely, cluster 1, cluster 5, cluster 6 and cluster 7, of which cluster 1 and cluster 6 had higher similarity, showing rapid growth rate in the early-stage but a tendency to slow down in the late-stage. In contrast to cluster 5 and cluster 7, which had slow growth rate in the early-stage and accelerated in the late-stage, and the four clusters belonged to the ascending type in terms of the overall trend, suggesting that the expression of this type of transcription factor kept on increasing with the reddening of the leaves. The second type belongs to descending type, with two clusters, namely cluster 2 and cluster 4, both of which showed a sharp decline in the early-stage and slowed down in the late-stage, but the declining trend of cluster 2 was much larger than that of cluster 4, indicating that the expression of differential genes belonging to these two clusters was getting lower and lower during leaf color change, and it was presumed that they were not the main cause for the colour change.

The third type belongs to ascending and then descending, with four clusters, namely cluster 3, cluster 8, cluster 9 and cluster 10. In this case, the rate of decline of clusters 9 and 10 is higher than that of clusters 3 and 8 at a late stage. Based on physiological assays of anthocyanoside content and metabolite accumulation, we hypothesized that the cause of these changes is likely to be related to the expression of the first type and third type cluster genes. Therefore, annotation analysis of transcription factors encoded by ascending (first type) and ascending-followed-by-descending (third type) types (Fig. 5B and C) showed that the predominant ones were C2H2, zn-clus, bZIP, WRKY, and NAC, which were positively correlated between their expression levels and the accumulation of anthocyanosides. Thus, we hypothesized that they might play an important role in regulating the colour change of the *A. griseum* leaves.

### 3.5. Transcription factor analysis

The pathway governing anthocyanin biosynthesis is well-established, with the regulation by transcription factors playing a pivotal role. To investigate the role of transcription factors in the synthesis of anthocyanosides in *A. griseum*, we performed statistical analyses of the differential transcription factors in each group, and the results are shown in Fig. 6. The transcription factors bZIP, MYB-related, WRKY, and bHLH, which are related to anthocyanoside synthesis, were annotated to different degrees. Statistical analysis of their differential expression in different subgroups showed that the numbers of bZIP in GvsHR, GvsR and HRvsR were 111, 121, and 8, respectively; the numbers of MYB-related were 69, 68, and 3, respectively; the numbers of WRKY were 54, 59, and 1, respectively; and the numbers of bHLH were 64, 60, and 2, respectively. the differential transcription factor annotation pie plots showed that C2H2, bZIP, and zn-clus occupied the top three places in the rankings, respectively, and their up- and down-regulation in each subgroup was analyzed. A total of 119 C2H2 (upward 89, downward 30), 111 bZIP (upward 78, downward 33), and 74 zn-clus (74 upward) in GvsHR; a total of 138 C2H2 (upward 107, downward 31), 121 bZIP (upward 88, downward 33), and 86 zn-clus in

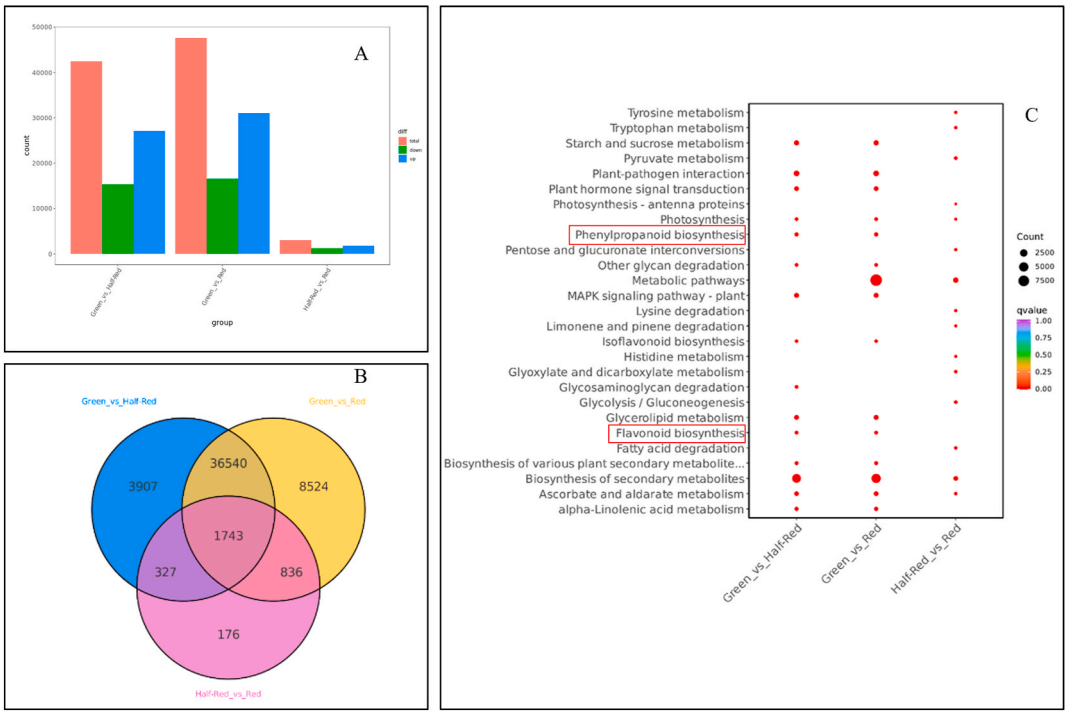


**Fig. 4.** The comparison of three different subgroups of differential genes in *A. griseum* leaves. a: up- and down-regulation of differential genes in each group A: Wayne's plot of differential genes in different subgroups; B: scatter plot of KEGG enrichment in multiple combinations.

GvsR (86 up-regulated); a total of 12 (10 up-regulated, 2 down-regulated) for C2H2, 8 (4 up-regulated, 4 down-regulated) for bZIP, and 12 (12 up-regulated) for zn-clus in HRvsR; that is to say, the expression levels of most of the three transcription factors, namely C2H2, bZIP, and zn-clus, were markedly increased in the half-red and the red periods, when compared with those in the green period, which was in accordance with the previous annotated results of Kmeans clustering analysis is also more consistent (Fig. 5). Thus, we speculated that C2H2 and bZIP also play an active role in the discolouration process of *A. griseum* leaves, and that they regulate and positively correlate with the accumulation of anthocyanosides, and that high expression during the half-red and red periods promotes the accumulation of anthocyanosides, which ultimately results in the bright red colour leaves.

### 3.6. Analysis of the expression levels of structural genes related to anthocyanin synthesis

Structural genes play a vital role in anthocyanin synthesis which is considered the primary driver of leaf reddening. Thus, we screened 191 genes related to anthocyanin synthesis from the transcriptome data, which were categorized into 12 structural genes and plotted a heatmap to visualize their expression levels at each period (Fig. 7B). Notably, 4 PAL genes, 5 CHS genes, 20 4CL genes, 1 C4H gene, 24 CHI genes, 10 F3H genes, 33 DFR genes, 1 f3′5′H gene, 2 ANS genes, 4 BZ1 genes, and 1 UFGT gene were more highly expressed during the half-red and full-red periods high. Overall, the expression of most of the genes increased with the reddening of the leaves, and in particular, the expression of the genes was much higher during the half-red and red periods than in the green leaf period, suggesting that these genes are likely to be involved in the metabolic activities of leaf colour change and play an active role in the accumulation of anthocyanin glycosides. We noted that the expression levels of the three FLS genes (Cluster-69534, Cluster-84663.0, and Cluster-99381.0) showed a decreasing trend with the accumulation of anthocyanosides.

### 3.7. Integration analysis of the transcriptome and metabolome and identification of the relevant transcription factors

To investigate the role played by regulatory genes in anthocyanin biosynthesis, we screened for differential transcription factors (Padj<0.05) and obtained a total of 35 transcription factors (Supplementary Table 7). Their correlations with differential metabolites were calculated, and the top 6 TFs with positive and negative correlations were selected for clustering heat map analysis, respectively (Fig. 8A). The results showed that there were strong correlations between these 12 transcription factors and differential metabolites. These transcription factors were classified into two groups according to the different correlations: the first group included bZIP 1, TiFY, zn-clus 7, TUB, bZIP 2, and NAC for a total of 6 TFs, which were associated with Peonidin-3-O-sophoroside, Malvidin-3-O-rutinoside, Peonidin-3- sophoroside-5-glucoside, Delphinidin-3-O-sambubioside, and Petunidin-3-O-arabinoside, and five metabolites showed strong negative correlations, whereas they showed strong positive correlations with the remaining 22 metabolites; the second group included C2C2-GATA 1, C2H2 10, C2C2-GATA 2, bHLH, HB-WOX, and LOB, a total of six transcription factors, whose positive and negative correlations with metabolites were the exact opposite of those of the first class of TFs: the positive and negative correlations with Peonidin-3-O-sophoroside, Malvidin-3-O-rutinoside, Peonidin-3- sophoroside-5-glucoside, Delphinidin-3-O-sambubioside, and Petunidin-3-O-arabinoside, and a strong positive correlation with the remaining 22 metabolites. The results of the changes in the accumulation amounts of the differential metabolites showed (Supplementary Table 8) that the contents of the latter 22 metabolites increased in the HR and R periods compared with the green period, and this trend was consistent with the trend of the anthocyanoside contents in the physiological index assay; therefore, we hypothesized that the first group of TFs played an important positive regulatory role in the synthesis of anthocyanosides of *A. griseum*.

Later, the correlation heat map analysis of these 12 TFs with structural genes (Fig. 8B) showed that they also had strong correlations with 25 structural genes. The second type of transcription factors were

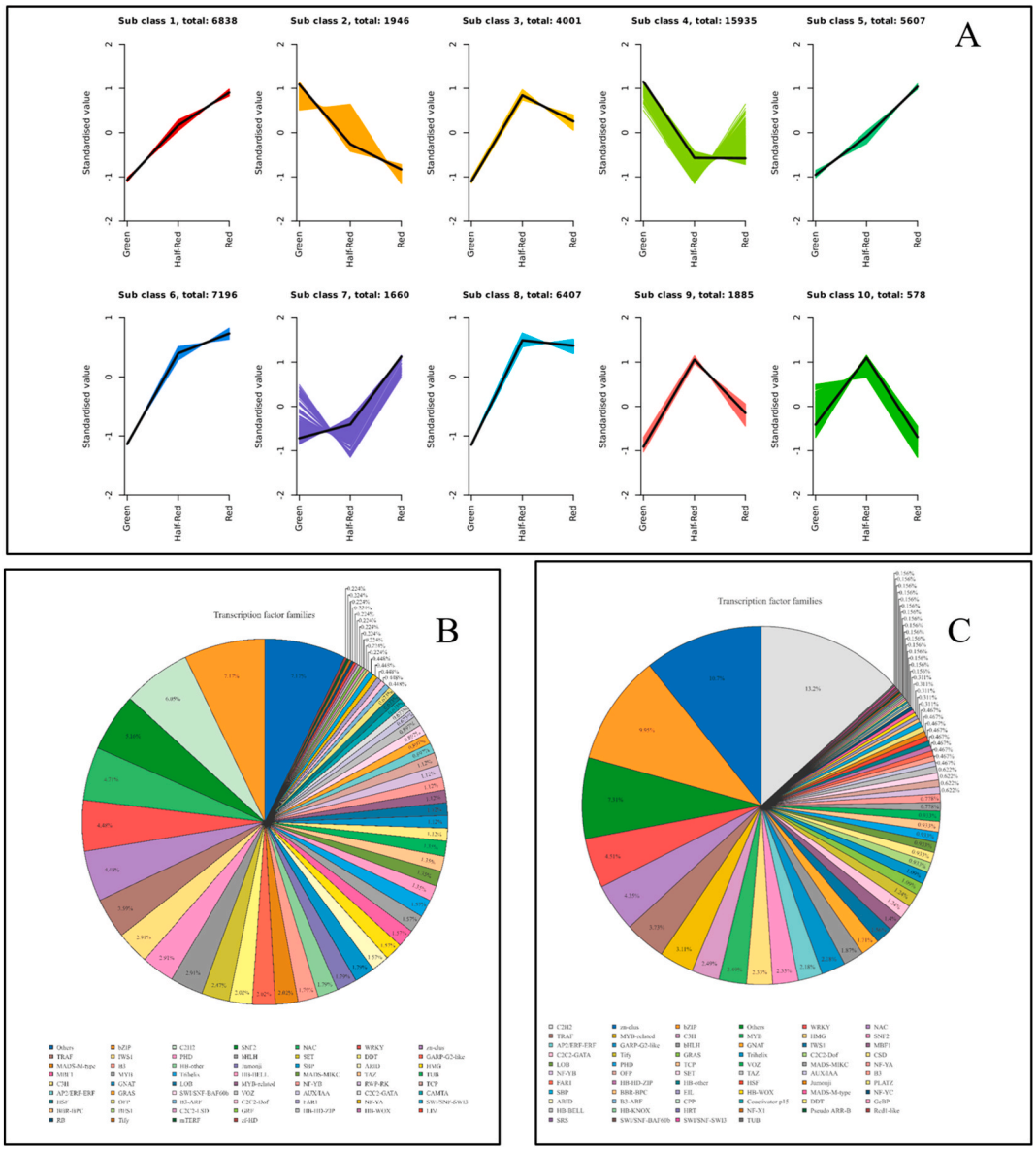


**Fig. 5.** The differential gene K-means analysis clusters and transcription factor annotation statistics. A: differential gene Kmeans clusters; B: ascending then descending type transcription factor annotation; C: ascending type transcription factor annotation.

negatively correlated with 15 structural genes, including FLS 2, BZ1 2, and F3H, and positively correlated with 10 genes, including DFR 2, F3H4, and DFR 1. Combined with the changes in the expression levels of these key structural genes in the three periods (Supplementary Table 9), we speculated that these 12 TFs either positively regulated or negatively regulated the changes in downstream structural genes, which caused the increase of the content of related metabolites, and ultimately led to the bright red color of the leaves.

### *3.8. Validation of gene expression using qRT-PCR*

To verify the accuracy of the transcriptome data, we selected 12 candidate genes and designed primers for fluorescence quantification experiments to detect their expression levels at the green, half-red and red stages (Fig. 9).

The 12 genes were classified into three types according to their expression: Cluster-104207.0, Cluster-100829.5, Cluster-105013.1, Cluster-69534.1 belonged to the first type, and their gene expression was highest in the green period; Cluster-85519.0, Cluster-89936.0, Cluster-84571.3 belong to the second kind, their gene expression is highest in the half-red period; Cluster-105999.3, Cluster-79986.0, Cluster-45977.12, Cluster-45977.9, Cluster- 80948.0 belonged to the third type, and their gene expression was highest in the red period. The results were consistent with the transcriptome data sand proved the reliability of the transcriptome data.

## 4. Discussion

### *4.1. Higher anthocyanin content is the main reason for the red colour transition by the leaves*

During autumn, the leaves of the *A. griseum* undergo a shift in color from green to vibrant red, with some variations depending on changes of the specific environmental conditions (light, temperature etc.) at their planting sites. Due to the different natural environments of the planting site, the transition process sometimes is different, such as some transition to orange and then to bright red, but ultimately most of them turn bright red at the end. Some studies have shown that leaf coloration is

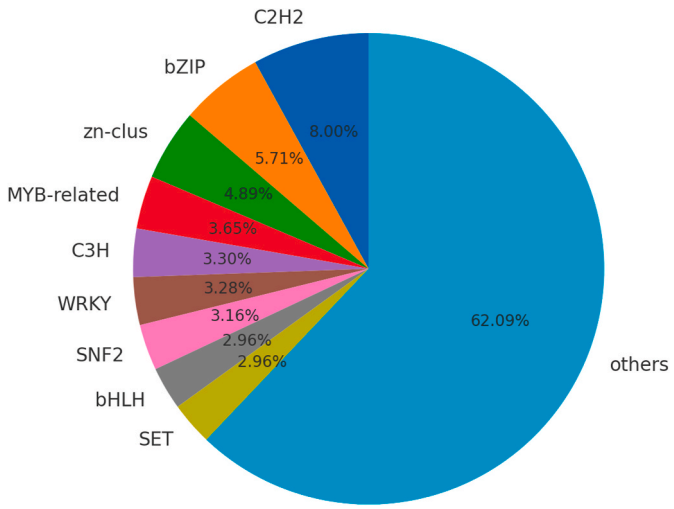


**Fig. 6.** Pie chart of the differential transcription factor annotations.

closely related to the levels of chlorophyll, carotenoids, and anthocyanin (Tian et al., 2019); and the content of chlorophyll *a* is the highest in the initial stage, which accounted for a larger proportion of the four substances, leading to the visual green coloration of the leaves in this stage. As temperatures decrease, chlorophyll degrades, leading to a significant decrease and the emergence of a bright red color (Azoulay Shemer et al., 2008; Menzies et al., 2016). While carotenoids also decline, their relative content increases, causing the leaves to turn yellow. In the subsequent stage, anthocyanin accumulates, resulting in a half-yellow, half-red appearance. In the final stage, the accumulation of total anthocyanin content increases and anthocyanosides occupy an absolute dominant position, resulting in the leaves appearing bright red. Recent research suggested that the increase of anthocyanin content in plants is the main reason for the red coloration of leaves (Ye et al., 2022), and our results strongly support this statement. It is noteworthy that the phenotypic and pigment content of the leaves changed significantly during the period from green to semi-red, as evidenced by a sharp decrease in chlorophyll and carotenoid content and an increasing anthocyanin content, suggesting that the changes in *A. griseum* were the most pronounced and the related gene expression and metabolites were the most abundant in this time period, which was later confirmed by the transcription and metabolism data.

### 4.2. Metabolomic analysis discovered various major anthocyanoside fractions

Research has demonstrated the significant role of cyanidin, a common anthocyanidin, in determining plant coloration (Fu et al., 2021). For instance, in crape myrtle, cyanidin and pelargonidin are identified as the primary anthocyanins responsible for color presentation.Two bHLH-regulated Cyanidin-3-O-glucoside accumulation leads to discolouration of *Phoebe bournei* leaves (Feng et al., 2024). We conducted a comparative analysis of metabolite data from leaves of *A. griseum* across three stages of color transition. Our study found a greater number of up-regulated metabolites during the color transition stages, with notably higher expression levels during the half-red and full-red phases compared to the green stage. Subgroup comparisons revealed that cyanidin, pelargonidin, and flavonoid were the major up-regulators compared to the green period (Fig. 3A and B). Comparison of the 44 differential metabolites (Fig. 8) showed an increase in 26 substances including 11 cyanidins, from which we hypothesized that cyanidins are the major component of *A. griseum* anthocyanosides. Ranking the different metabolites in each group by $\log_2$FC value showed that Cyanidin-3,5-O-diglucoside had the largest multiplicative difference compared with the green period (Supplementary Fig. 1), indicating that the content of this metabolite varied the most significantly, and accumulated the most during the green to half-red period, and that its

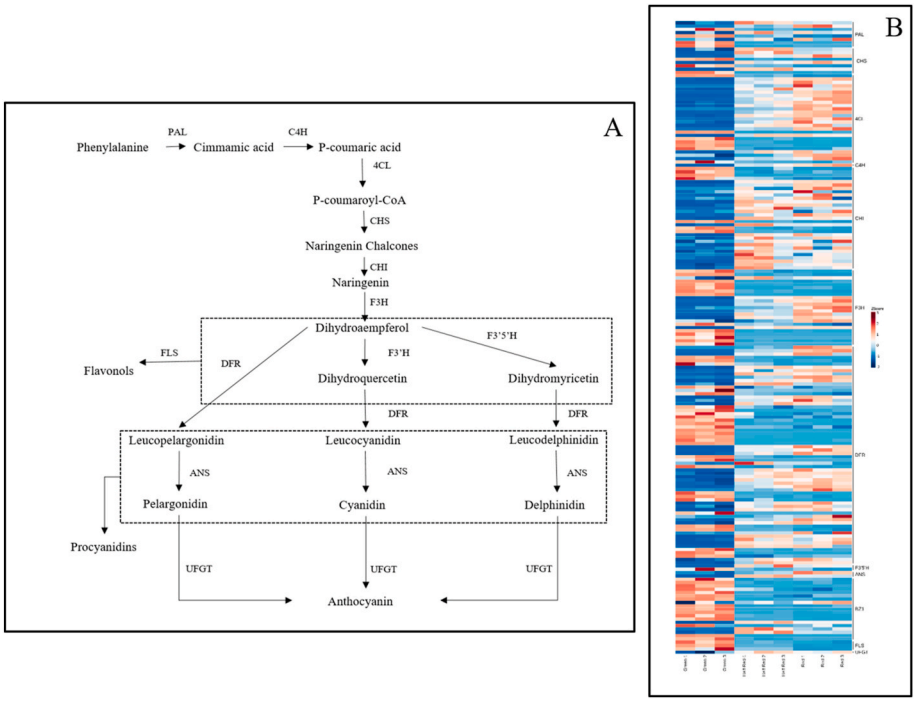


**Fig. 7.** Regulation of genes of phenylpropanoid, flavonoid and anthocyanin biosynthesis pathways during leaf colour changes in *A. griseum*. A: Synthesis of anthocyanosides in *A. griseum*. B: Heatmaps show down- and up-regulated structural genes. PAL, phenylalanine ammonia-lyase; C4H, cinnamate 4-hydroxylase; 4CL, 4-coumarate CoA ligase; CHS, chalcone synthase; CHI, chalcone isomerase; DFR, dihydroflavonol 4-reductase; F3H, flavanone 3-hydroxylase; F3′H, flavonoid 3′-hydroxylase; F3′5′H, flavonoid-3′,5′-hydroxylase; FLS, flavonol synthase ANS, anthocyanidin synthase; UFGT, UDP glucose-flavonoid 3-O-glcosyl-transferase; BZ1, anthocyanidin 3-O-glucosyltransferase.

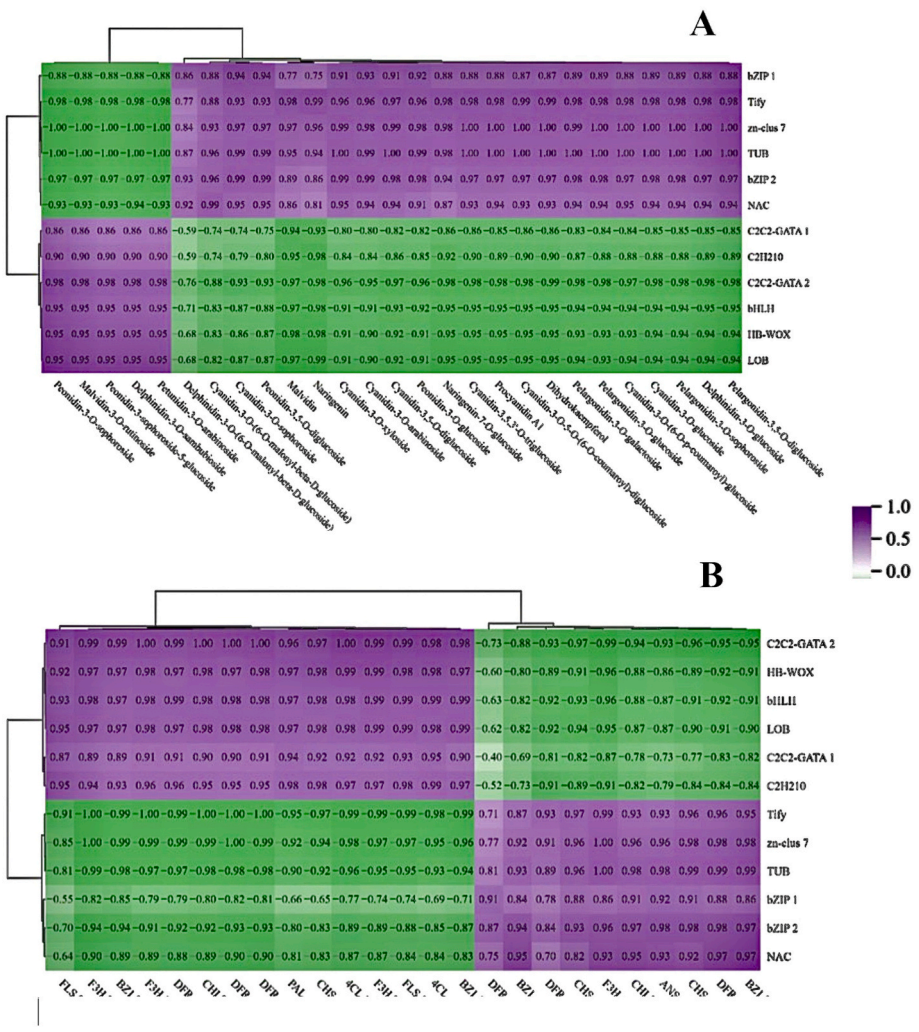


**Fig. 8.** The 12 key transcription factor (TF) clustering heatmaps A:TF correlation with differential metabolites clustering heatmap B:TF correlation analysis with structural genes.

content had a very close relationship with the coloration of the leaves. Our results demonstrated that cyanidin, particularly Cyanidin-3, 5-O-diglucoside, serves as the primary metabolite responsible for the reddening of *A. griseum* leaves.

### *4.3. Changes in structural genes and transcription factors affect anthocyanin biosynthesis*

Anthocyanidin synthesis originates from the metabolism of phenylpropane, and the genes encoding PAL, C4H and 4CL, as the key genes in the metabolism of phenylpropane (Dong and Lin, 2021), play an important promotional role in anthocyanidin synthesis, and their expression levels are significantly increased in the half-red and red periods, which accumulates a higher amount of substrate for the synthesis of anthocyanidin in *A. griseum*. CHS, CHI, F3H, etc. are indispensable and important genes in the anthocyanin metabolic pathway, and the amount of their expression will directly affect the content of metabolites. In this experiment, 191 genes related to anthocyanin synthesis were screened from the transcriptome data, and they were categorized into 12 s structural genes (Fig. 7B). The expression of these genes was increased during the half-red and full-red periods, and the metabolites were increased by the catalysis of various enzymes, which ultimately resulted in the formation of more colourless anthocyanins, which were catalyzed into colored anthocyanins by dehydrogenation, isomerization, and dehydration of the ANS genes under acidic conditions (Shi and Xie, 2014). UFGT, as a downstream gene in the anthocyanin biosynthesis pathway, is responsible for the conversion of the unstable anthocyanidins into relatively stable anthocyanin-3-O-glucosides (Muhammad et al., 2022), the expression trend of UFGT gene in lychee was positively correlated with the content of anthocyanidins in the pericarp, and heterologous expression of UFGT in tobacco resulted in an increase of anthocyanidin content in tobacco (Zhao et al., 2012). Therefore, it is hypothesized that during the process of *A. griseum* leaf colour transition, all 11 structural genes represented by ANS and UFGT were significantly up-regulated in their expression during the half-red and full-red periods of the leaves, which caused the accumulation of anthocyanins and led to the reddening of *A. griseum* leaf colour. In addition to the up-regulated structural genes, we also observed that the expression levels of the three FLS genes showed a decreasing trend with the accumulation of anthocyanins, and speculated that it might be the case that DFR and FLS competed for dihydroquercetin as a substance together, and that the two were in competition with each other, and the increase in the expression level of DFR implied that more dihydroquercetin was converted into colourless anthocyanins, and more anthocyanins were eventually produced.

In addition to the structural genes, regulatory genes also have important roles in anthocyanin synthesis (He et al., 2023). In our data, a total of 12 key TFs including bZIP, TiFY, zn-clus 7, TUB, NAC, C2C2-GATA, C2H2, bHLH, HB-WOX, and LOB were identified by correlation calculations of differential transcription factors and differential

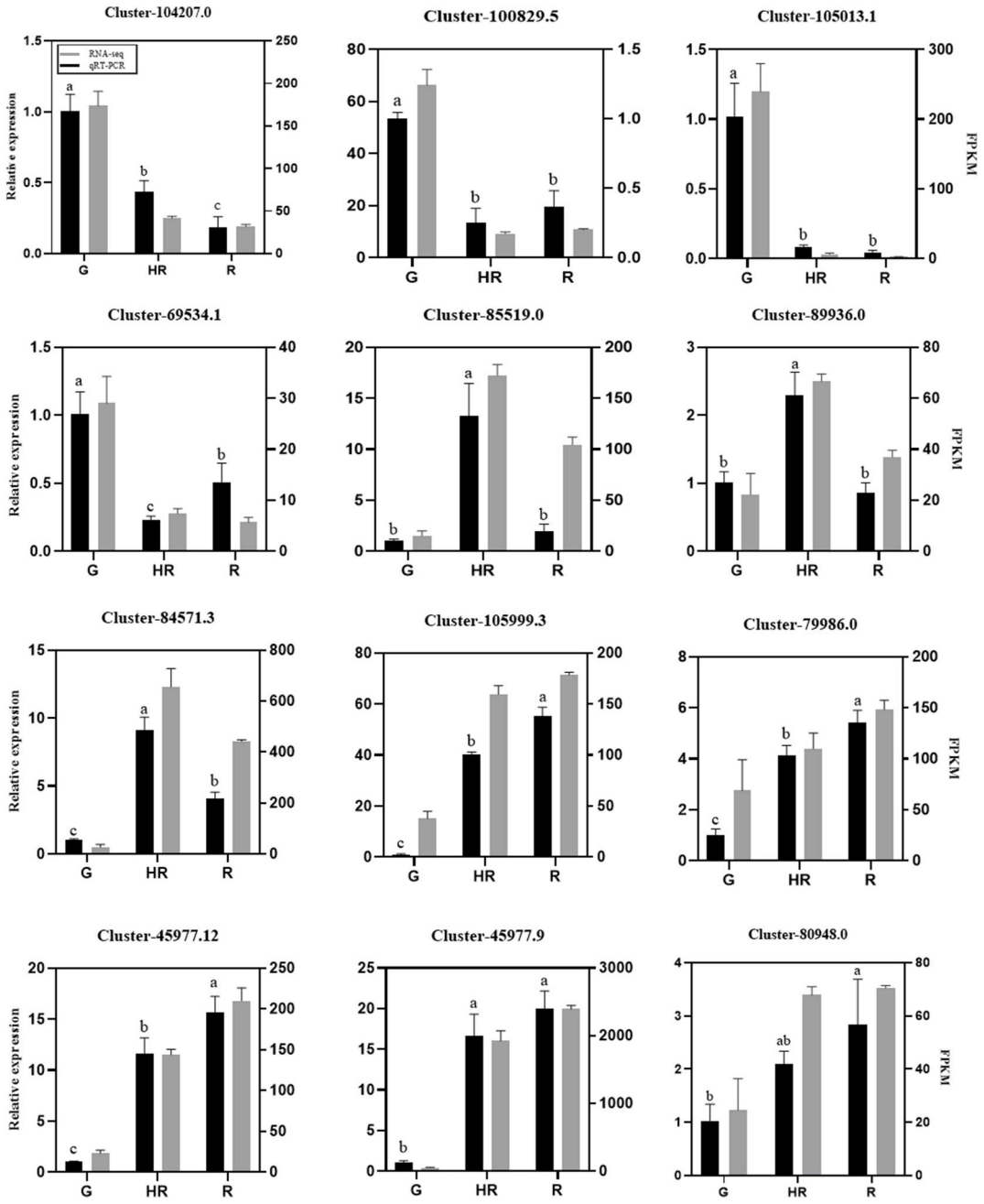


**Fig. 9.** The qRT-PCR validation of expression levels of 12 DEGs identified by RNA sequencing. The left y-axis indicates the relative gene expression level ($2^{-\Delta\Delta Ct}$) analyzed by qRT-PCR; the right y-axis shows the FPKM values obtained by RNA-seq. x-axis indicates leaf samples at 3 stages. Bars with different letters are significantly different ($p < 0.05$). G, green period; HR, half-red period; R, red period.

metabolites. cmNAC25 in chrysanthemum was reported to positively regulate the synthesis of anthocyanosides through direct activation of CmMYB6 and CmDFR, positively regulates anthocyanin biosynthesis in chrysanthemum petals (Wang et al., 2023); and the C2H2 transcription factor family in azalea dominates the anthocyanin-related hierarchical gene regulation, which results in red coloration of azalea petals (Nie et al., 2023). From this, we hypothesized that these 12 TFs play an important regulatory role in anthocyanoside biosynthesis in blood maple. However, the same TFs have variability among different species and may be positive or negative regulators, which need to be analyzed species-specifically. For example, PgbZIP16 and PgbZIP34 were found to be homologous to *Arabidopsis* AtHY5 and AtHYH in the pomegranate genome, which are highly expressed in safflower petals to promote anthocyanidin accumulation (Wang et al., 2022); whereas in grapevine, an allele of VvbZIP36 was knocked down using CRISPR/Cas9, and comparing with the wild type, the mutant in which a series of anthocyanin biosynthesis genes were activated, leading to the accumulation of related metabolites such as naringenin, dihydroflavonols and anthocyanin-3- O-glucoside (Tu et al., 2022). The six TFs represented by bZIP in *A. griseum* showed a clear positive correlation with the rising 22 differential metabolites, and it is hypothesized that they are positive regulators of anthocyanoside synthesis in *A. griseum*, while in contrast, the six TFs represented by C2H2 are negative regulators (Fig. 8). Their changes in the middle and late stages of colour change were either activated or repressed the expression levels of related structural genes such as DFR, BZ1, and ANS, resulting in a significant increase in anthocyanoside content and more pronounced differences in leaf phenotypes during these two periods.

## 5. Conclusion

In conclusion, our study provided comprehensive insights into the physiological and molecular mechanisms governing leaf color changes in *Acer griseum*, a species valued for its ornamental attributes and ecological significance. Through integrated physiological, transcriptional, and metabolic analyses, we demonstrated that the accumulation of anthocyanidins, particularly cyanidin-3,5-O-diglucoside, regulated the transition from green to red autumn foliage, with significant changes occurring during the half-red stage. Correlation analysis showed that the 12 key TFs were significantly correlated with anthocyanin-related metabolites and structural genes, contributing important regulatory roles duringthe biosynthesis of anthocyanosides in *A. griseum*. These observations enhanced our current understanding of the genetic basis underlying leaf color variation in *A. griseum*, offering valuable insights for further targeted genetic breeding and conservation efforts of this endemic and endangered species.

## Author contributions

**Huizhen Fan:** Experiments to obtain data, data processing and analysis, completion of the first draft of the thesis; **Huimin Liao:** Supporting experiments, partial data processing; **Yingxue Shen:** Sample acquisition, processing, and preservation; **Md. Nasir Hossain Sani:** Provided some advice on parts of the thesis. Assisted in the review, editing and linguistic presentation of the manuscript in English; **Jean Wan Hong Yong:** Reviewed the manuscript of the pape, made critical and constructive revisions, additional funding; **Junyang Song:** Selection of topic, experimental design, guidance of experimental process, provision of thesis framework structure, guidance of thesis writing, revision of the first draft of the thesis, review of the final draft of the thesis.

## Funding

This research was funded by the Department of Science and Technology of Shaanxi Province (2024NC-YBXM-072), Education Department of Shaanxi Provincial government, Institute for Basic Science Research (IBSR) project.

## Declaration of competing interest

The authors declare that they have no known competing financial interests or personal relationships that could have appeared to influence the work reported in this paper.

## Acknowledgments

We would like to express our gratitude to the Northwest A&F University (China) and the Swedish University of Agricultural Sciences (Sweden) for providing the research infrastructures and various other support towards this inter-university collaborative research activity.

## Appendix A. Supplementary data

Supplementary data to this article can be found online at https://doi.org/10.1016/j.plaphy.2024.109198.

## Data availability

Data will be made available on request.

## References

Alappat, B., Alappat, J., 2020. Anthocyanin pigments: beyond aesthetics. Molecules 25 (23), 5500.

An, J.P., Yao, J.F., Xu, R.R., You, C.X., Wang, X.F., Hao, Y.J., 2018. Apple bZIP transcription factor MdbZIP44 regulates abscisic acid-promoted anthocyanin accumulation. Plant Cell Environ. 41 (11), 2678–2692. https://doi.org/10.1111/pce.13393.

An, J.P., Zhang, X.W., Bi, S.Q., You, C.X., Wang, X.F., Hao, Y.J., 2020. The ERF transcription factor MdERF38 promotes drought stress-induced anthocyanin biosynthesis in apple. Plant J. : cell molec. biol. 101 (3), 573–589. https://doi.org/10.1111/tpj.14555.

Azarin, K., Usatov, A., Minkina, T., Duplii, N., Fedorenko, A., Plotnikov, A., Mandzhieva, S., Kumar, R., Yong, J.W.H., Sehar, S., Rajput, V.D., 2024. Evaluating the phytotoxicological effects of bulk and nano forms of zinc oxide on cellular respiration-related indices and differential gene expression in *Hordeum vulgare* L. Ecotoxicol. Environ. Saf. 282, 116670. https://doi.org/10.1016/j.ecoenv.2024.116670.

Azoulay Shemer, T., Harpaz-Saad, S., Belausov, E., Lovat, N., Krokhin, O., Spicer, V., Standing, K.G., Goldschmidt, E.E., Eyal, Y., 2008. Citrus chlorophyllase dynamics at ethylene-induced fruit color-break: a study of chlorophyllase expression, posttranslational processing kinetics, and *in situ* intracellular localization. Plant Physiol. 148 (1), 108–118. https://doi.org/10.1104/pp.108.124933.

Chang, Y.Q., Tan, S.N., Yong, J.W.H., Ge, L., 2011. Surfactant assisted pressurized liquid extraction for determination of flavonoids from *Costus speciosus* by micellar electrokinetic chromatography. J. Separ. Sci. 34, 462–469. https://doi.org/10.1002/jssc.201000766.

Chen, Y.S., Chesson, P., Wu, H.W., Pao, S.H., Liu, J.W., Chien, L.F., Yong, J.W.H., Sheue, C.R., 2017. Leaf structure affects a plant's appearance: combined multiple-mechanisms intensify remarkable foliar variegation. J. Plant Res. 130, 311–325. https://doi.org/10.1007/s10265-016-0890-4.

Chen, L., Hu, B., Qin, Y., Hu, G., Zhao, J., 2019. Advance of the negative regulation of anthocyanin biosynthesis by MYB transcription factors. Plant Physiol. Biochem. : PPB (Plant Physiol. Biochem.) 136, 178–187. https://doi.org/10.1016/j.plaphy.2019.01.024.

Chen, L., Huang, Y., Xu, M., Cheng, Z., Zheng, J., 2017. Proteomic analysis reveals coordinated regulation of anthocyanin biosynthesis through signal transduction and sugar metabolism in black rice leaf. Int. J. Mol. Sci. 18 (12), 2722.

Dong, N.Q., Lin, H.X., 2021. Contribution of phenylpropanoid metabolism to plant development and plant-environment interactions. J. Integr. Plant Biol. 63 (1), 180–209. https://doi.org/10.1111/jipb.13054.

Duan, A.Q., Deng, Y.J., Tan, S.S., Xu, Z.S., Xiong, A.S., 2023. A MYB activator, DcMYB11c, regulates carrot anthocyanins accumulation in petiole but not taproot. Plant Cell Environ. 46 (9), 2794–2809. https://doi.org/10.1111/pce.14653.

Espley, R.V., Jaakola, L., 2023. The role of environmental stress in fruit pigmentation. Plant Cell Environ. 46, 3663–3679. https://doi.org/10.1111/pce.14684.

Feng, L., Shen, P., Chi, X., Zhou, Y., Liu, J., Cheng, T., Wang, J., Zhang, Q., Cai, M., Pan, H., 2024. The anthocyanin formation of purple leaf is associated with the activation of LfiHY5 and LfiMYB75 in crape myrtle. Horticult. Plant J. 10 (5), 1230–1246. https://doi.org/10.1016/j.hpj.2023.02.016.

Fu, M., Yang, X., Zheng, J., Wang, L., Yang, X., Tu, Y., Ye, J., Zhang, W., Liao, Y., Cheng, S., Xu, F., 2021. Unraveling the regulatory mechanism of color diversity in *Camellia japonica* petals by integrative transcriptome and metabolome analysis. Front. Plant Sci. 12, 685136. https://doi.org/10.3389/fpls.2021.685136.

Gao, J., Sun, X., Zong, Y., Yang, S., Wang, L., Liu, B., 2020. Functional MYB transcription factor gene HtMYB2 is associated with anthocyanin biosynthesis in *Helianthus tuberosus* L. BMC Plant Biol. 20 (1), 247. https://doi.org/10.1186/s12870-020-02463-8.

Ge, L., Yong, J.W.H., Tan, S.N., Hua, L., Ong, E.S., 2008. Analyses of gibberellins in coconut water by partial filling - micellar electrokinetic chromatography - mass spectrometry with reversal of electroosmotic flow. Electrophoresis 29. https://doi.org/10.1002/elps.200700717, 2032-2126.

Gibbs, D., Chen, Y., 2009. The red list of maples. Botanic Gardens Conser. Intern. 7.

Hao, Z., Liu, S., Hu, L., Shi, J., Chen, J., 2020. Transcriptome analysis and metabolic profiling reveal the key role of carotenoids in the petal coloration of *Liriodendron tulipifera*. Hortic. Res. 7, 70. https://doi.org/10.1038/s41438-020-0287-3.

He, A., Ma, Z., Li, Y, Huang, C., Yong, J.W.H., Huang, J., 2023. Spatiotemporal, physiological and transcriptomic dynamics of wild jujube seedlings under saline conditions. Tree Physiol 43, 832–850. https://doi.org/10.1093/treephys/tpad001.

He, F., Mu, L., Yan, G.L., Liang, N.N., Pan, Q.H., Wang, J., Reeves, M.J., Duan, C.Q., 2010. Biosynthesis of anthocyanins and their regulation in colored grapes. Molecules 15 (12), 9057–9091. https://doi.org/10.3390/molecules15129057.

He, G., Zhang, R., Jiang, S., Wang, H., Ming, F., 2023. The MYB transcription factor RcMYB1 plays a central role in rose anthocyanin biosynthesis. Hortic. Res. 10 (6), uhad080. https://doi.org/10.1093/hr/uhad080.

Heng, M.Y., Tan, S.N., Yong, J.W.H., Ong, E.S., 2013. Emerging green technologies for the chemical standardization of botanicals and herbal preparations. Trends Anal. Chem. 50, 1–11. https://doi.org/10.1016/j.trac.2013.03.012.

Hong, Y., Yang, L.W., Li, M.L., Dai, S.L., 2016. Comparative analyses of light-induced anthocyanin accumulation and gene expression between the ray florets and leaves in chrysanthemum. Plant Physiol. Biochem. 103, 120–132. https://doi.org/10.1016/j.plaphy.2016.03.006.

Hughes, N.M., Lev-Yadun, S., 2023. Review: Why do some plants have leaves with red or purple undersides? Environ. Exp. Bot. 205, 105126. https://doi.org/10.1016/j.envexpbot.2022.105126.

Inácio, M.R., de Lima, K.M., Lopes, V.G., Pessoa, J.D., de Almeida Teixeira, G.H., 2013. Total anthocyanin content determination in intact açaí (Euterpe oleracea Mart.) and palmitero-juçara (Euterpe edulis Mart.) fruit using near infrared spectroscopy (NIR) and multivariate calibration. Food Chem. 136 (3–4), 1160–1164. https://doi.org/10.1016/j.foodchem.2012.09.046.

Karppinen, K., Lafferty, D.J., Albert, N.W., Mikkola, N., McGhie, T., Allan, A.C., Afzal, B. M., Häggman, H., Espley, R.V., Jaakola, L., 2021. MYBA and MYBPA transcription factors co-regulate anthocyanin biosynthesis in blue-coloured berries. New Phytol. 232 (3), 1350–1367. https://doi.org/10.1111/nph.17669.

Kim, D.H., Park, S., Lee, J.Y., Ha, S.H., Lim, S.H., 2018. Enhancing flower color through simultaneous expression of the B-Peru and mPAP1 transcription factors under control of a flower-specific promoter. Int. J. Mol. Sci. 19 (1). https://doi.org/10.3390/ijms19010309.

Lev-Yadun, S., 2022. The phenomenon of red and yellow autumn leaves: hypotheses, agreements and disagreements. J. Evol. Biol. 35, 1245–1282. https://doi.org/10.1111/jeb.14069.

Li, W., Li, H., Shi, L., Shen, P., Li, Y., 2022. Leaf color formation mechanisms in *Alternanthera bettzickiana* elucidated by metabolite and transcriptome analyses. Planta 255, 59. https://doi.org/10.1007/s00425-022-03840-3.

Li, C., Shi, L., Li, X., Wang, Y., Bi, Y., Li, W., Ma, H., Chen, B., Zhu, L., Fu, Y., 2022. ECAP is a key negative regulator mediating different pathways to modulate salt stress-induced anthocyanin biosynthesis in Arabidopsis. New Phytol. 233 (5), 2216–2231. https://doi.org/10.1111/nph.17937.

Li, C., Wu, J., Hu, K.D., Wei, S.W., Sun, H.Y., Hu, L.Y., Han, Z., Yao, G.F., Zhang, H., 2020. PyWRKY26 and PybHLH3 cotargeted the PyMYB114 promoter to regulate anthocyanin biosynthesis and transport in red-skinned pears. Hortic. Res. 7, 37. https://doi.org/10.1038/s41438-020-0254-z.

Li, H., Wang, S., Zhai, L., Cui, Y., Tang, G., Huo, J., Li, X., Bian, S., 2024. The miR156/SPL12 module orchestrates fruit colour change through directly regulating ethylene production pathway in blueberry. Plant Biotechnol. J. 22 (2), 386–400. https://doi.org/10.1111/pbi.14193.

Liu, F., Zhao, P., Chen, G., Wang, Y., Yang, Y., 2023. A comparative analysis of small RNA sequencing data in tubers of purple potato and its red mutant reveals small RNA regulation in anthocyanin biosynthesis. PeerJ 11, e15349. https://doi.org/10.7717/peerj.15349.

Liu, R., Lai, B., Hu, B., Yonghua, Q., Hu, G., Zhao, J., 2017. Identification of MicroRNAs and their target genes related to the accumulation of anthocyanins in *Litchi chinensis* by high-throughput sequencing and degradome analysis. Front. Plant Sci. 7. https://doi.org/10.3389/fpls.2016.02059.

Liu, Y., Tikunov, Y., Schouten, R.E., Marcelis, L.F.M., Visser, R.G.F., Bovy, A., 2018. Anthocyanin biosynthesis and degradation mechanisms in solanaceous vegetables: a review. Front. Chem. 6, 52. https://doi.org/10.3389/fchem.2018.00052.

Long, L., Liu, J., Gao, Y., Xu, F.C., Zhao, J.R., Li, B., Gao, W., 2019. Flavonoid accumulation in spontaneous cotton mutant results in red coloration and enhanced disease resistance. Plant Physiol. Biochem. : PPB (Plant Physiol. Biochem.) 143, 40–49. https://doi.org/10.1016/j.plaphy.2019.08.021.

Lu, X., Chen, Z., Gao, J., Fu, S., Hu, H., Ren, J., 2020. Combined metabolome and transcriptome analyses of photosynthetic pigments in red maple. Plant Physiol. Biochem. 154, 476–490. https://doi.org/10.1016/j.plaphy.2020.06.025.

Ma, Z., He, A., Han, Q., Zhao, X., Yong, J.W.H., Huang, J., 2022. Mycorrhizal symbiosis in jujube enhances salt tolerance by altering ion fluxes and fatty acid metabolism. Plant Physiol. 189, 2481–2499. https://doi.org/10.1093/plphys/kiac239.

Ma, M., Liu, Y., Bai, C., Yang, Y., Sun, Z., Liu, X., Zhang, S., Han, X., Yong, J.W.H., 2021. The physiological functionality of PGR5/PGRL1-dependent cyclic electron transport in sustaining photosynthesis. Front. Plant Sci. 12, 702196. https://doi.org/10.3389/fpls.2021.702196.

Mei, X., Lin, C., Wan, S., Chen, B., Wu, H., Zhang, L., 2021. A comparative metabolomic analysis reveals difference manufacture suitability in "yinghong 9" and "huangyu" teas (Camellia sinensis). Front. Plant Sci. 12, 767724. https://doi.org/10.3389/fpls.2021.767724.

Menzies, I.J., Youard, L.W., Lord, J.M., Carpenter, K.L., van Klink, J.W., Perry, N.B., Schaefer, H.M., Gould, K.S., 2016. Leaf colour polymorphisms: a balance between plant defence and photosynthesis. J. Ecol. 104, 104–113. https://doi.org/10.1111/1365-2745.12494.

Morita, Y., Saitoh, M., Hoshino, A., Nitasaka, E., Iida, S., 2006. Isolation of cDNAs for R2R3-MYB, bHLH and WDR transcriptional regulators and identification of c and ca mutations conferring white flowers in the Japanese morning glory. Plant Cell Physiol. 47 (4), 457–470. https://doi.org/10.1093/pcp/pcj012.

Muhammad, N., Luo, Z., Yang, M., Li, X., Liu, Z., Liu, M., 2022. The joint role of the late anthocyanin biosynthetic UFGT-encoding genes in the flowers and fruits coloration of horticultural plants. Sci. Hortic. 307. https://doi.org/10.1016/j.scienta.2022.111110.

Naing, A.H., Kim, C.K., 2021. Abiotic stress-induced anthocyanins in plants: their role in tolerance to abiotic stresses. Physiol. Plantarum 172 (3), 1711–1723. https://doi.org/10.1111/ppl.13373.

Nie, S., Zhao, S.W., Shi, T.L., Zhao, W., Zhang, R.G., Tian, X.C., Guo, J.F., Yan, X.M., Bao, Y.T., Li, Z.C., Kong, L., Ma, H.Y., Chen, Z.Y., Liu, H., El-Kassaby, Y.A., Porth, I., Yang, F.S., Mao, J.F., 2023. Gapless genome assembly of azalea and multi-omics investigation into divergence between two species with distinct flower color. Hortic. Res. 10 (1), uhac241. https://doi.org/10.1093/hr/uhac241.

Qin, L., Sun, L., Wei, L., Yuan, J., Kong, F., Zhang, Y., Miao, X., Xia, G., Liu, S., 2021. Maize SRO1e represses anthocyanin synthesis through regulating the MBW complex in response to abiotic stress. Plant J. : cell molec. biol. 105 (4), 1010–1025. https://doi.org/10.1111/tpj.15083.

Shan, X., Li, Y., Yang, S., Gao, R., Zhou, L., Bao, T., Han, T., Wang, S., Gao, X., Wang, L., 2019. A functional homologue of Arabidopsis TTG1 from Freesia interacts with bHLH proteins to regulate anthocyanin and proanthocyanidin biosynthesis in both *Freesia* hybrida and *Arabidopsis thaliana*. Plant Physiol. Biochem. : PPB (Plant Physiol. Biochem.) 141, 60–72. https://doi.org/10.1016/j.plaphy.2019.05.015.

Shao, D., Li, Y., Zhu, Q., Zhang, X., Liu, F., Xue, F., Sun, J., 2021. GhGSTF12, a glutathione S-transferase gene, is essential for anthocyanin accumulation in cotton (*Gossypium hirsutum* L.). Plant Sci. : Intern. J. experi. plant biol. 305, 110827. https://doi.org/10.1016/j.plantsci.2021.110827.

Sheue, C.R., Sarafis, V., Kiew, R., Liu, H.Y., Salino, A., Kuo-Huang, L.L., Yang, Y.P., Tsai, C.C., Lin, C.H., Yong, J.W.H., Ku, M.S.B., 2007. Bizonoplast, a unique chloroplast in the epidermal cells of microphylls in the shade plant *Selaginella erythropus* (Selaginellaceae). Am. J. Bot. 94, 1922–1929. https://doi.org/10.3732/ajb.94.12.1922.

Shi, M.Z., Xie, D.Y., 2014. Biosynthesis and metabolic engineering of anthocyanins in Arabidopsis thaliana. Recent Pat. Biotechnol. 8 (1), 47–60. https://doi.org/10.2174/1872208307666131218123538.

Teo, C.C., Tan, S.N., Yong, J.W.H., Ra, T., Liew, P., Ge, L., 2011. Metabolomics analysis of major metabolites in medicinal herbs. Anal. Methods 3, 2898–2908. https://doi.org/10.1039/C1AY05334E.

Tian, Y., Wang, H., Sun, P., Fan, Y., Qiao, M., Zhang, L., Zhang, Z., 2019. Response of leaf color and the expression of photoreceptor genes of Camellia sinensis cv. Huangjinya to different light quality conditions. Sci. Hortic. 251, 225–232. https://doi.org/10.1016/j.scienta.2019.03.032.

Tu, M., Fang, J., Zhao, R., Liu, X., Yin, W., Wang, Y., Wang, X., Wang, X., Fang, Y., 2022. CRISPR/Cas9-mediated mutagenesis of VvbZIP36 promotes anthocyanin accumulation in grapevine (Vitis vinifera). Hortic. Res. 9. https://doi.org/10.1093/hr/uhac022.

Walter, J., Kromdijk, J., 2022. Here comes the sun: How optimization of photosynthetic light reactions can boost crop yields. J. Integr. Plant Biol. 64, 564–591. https://doi.org/10.1111/jipb.13206.

Wang, F., Ji, G., Xu, Z., Feng, B., Zhou, Q., Fan, X., Wang, T., 2021. Metabolomics and transcriptomics provide insights into anthocyanin biosynthesis in the developing grains of purple wheat (*Triticum aestivum* L.). J. Agric. Food Chem. 69 (38), 11171–11184. https://doi.org/10.1021/acs.jafc.1c01719.

Wang, S., Zhang, X., Li, B., Zhao, X., Shen, Y., Yuan, Z., 2022. Genome-wide identification and characterization of bZIP gene family and cloning of candidate genes for anthocyanin biosynthesis in pomegranate (Punica granatum). BMC Plant Biol. 22 (1), 170. https://doi.org/10.1186/s12870-022-03560-6.

Wang, Y., Wang, Y., Zhou, L.J., Peng, J., Chen, C., Liu, S., Song, A., Jiang, J., Chen, S., Chen, F., 2023. CmNAC25 targets CmMYB6 to positively regulate anthocyanin biosynthesis during the post-flowering stage in chrysanthemum. BMC Biol. 21 (1), 211. https://doi.org/10.1186/s12915-023-01719-7.

Winkel-Shirley, B., 2001. Flavonoid biosynthesis. A colorful model for genetics, biochemistry, cell biology, and biotechnology. Plant Physiol. 126 (2), 485–493. https://doi.org/10.1104/pp.126.2.485.

Xu, Z., Wang, J., Ma, Y., Wang, F., Wang, J., Zhang, Y., Hu, X., 2023. The bZIP transcription factor SlAREB1 regulates anthocyanin biosynthesis in response to low temperature in tomato. Plant J. : cell molec. biol. 115 (1), 205–219. https://doi.org/10.1111/tpj.16224.

Yan, Y., Zhao, J., Lin, S., Li, M., Liu, J., Raymond, O., Vergne, P., Kong, W., Wu, Q., Zhang, X., Bao, M., Bendahmane, M., Fu, X., 2023. Light-mediated anthocyanin biosynthesis in rose petals involves a balanced regulatory module comprising transcription factors RhHY5, RhMYB114a, and RhMYB3b. J. Exp. Bot. 74 (18), 5783–5804. https://doi.org/10.1093/jxb/erad253.

Ye, S., Hua, S., Ma, T., Ma, X., Chen, Y., Wu, L., Zhao, L., Yi, B., Ma, C., Tu, J., Shen, J., Fu, T., Wen, J., 2022. Genetic and multi-omics analyses reveal BnaA07.PAP2In-184-317 as the key gene conferring anthocyanin-based color in Brassica napus flowers. J. Exp. Bot. 73 (19), 6630–6645. https://doi.org/10.1093/jxb/erac312.

Zhang, J., Li, S., An, H., Zhang, X., Zhou, B., 2022. Integrated transcriptome and metabolome analysis reveals the anthocyanin biosynthesis mechanisms in blueberry (*Vaccinium corymbosum* L.) leaves under different light qualities. Front. Plant Sci. 13, 1073332. https://doi.org/10.3389/fpls.2022.1073332.

Zhang, Y., Chen, C., Cui, Y., Du, Q., Tang, W., Yang, W., Kou, G., Tang, W., Chen, H., Gong, R., 2023. Potential regulatory genes of light induced anthocyanin accumulation in sweet cherry identified by combining transcriptome and metabolome analysis. Front. Plant Sci. 14. https://doi.org/10.3389/fpls.2023.1238624.

Zhao, Z.C., Hu, G.B., Hu, F.C., Wang, H.C., Yang, Z.Y., Lai, B., 2012. The UDP glucose: flavonoid-3-O-glucosyltransferase (UFGT) gene regulates anthocyanin biosynthesis in litchi (*Litchi chinesis* Sonn.) during fruit coloration. Mol. Biol. Rep. 39 (6), 6409–6415. https://doi.org/10.1007/s11033-011-1303-3.

Zhu, J., Wang, Y., Wang, Q., Li, B., Wang, X., Zhou, X., Zhang, H., Xu, W., Li, S., Wang, L., 2023. The combination of DNA methylation and positive regulation of anthocyanin biosynthesis by MYB and bHLH transcription factors contributes to the petal blotch formation in Xibei tree peony. Horticulture Res. 10 (7). https://doi.org/10.1093/hr/uhad100.